

Supplement of Hydrol. Earth Syst. Sci., 21, 4533–4549, 2017
<https://doi.org/10.5194/hess-21-4533-2017-supplement>
© Author(s) 2017. This work is distributed under
the Creative Commons Attribution 3.0 License.



Supplement of

Recent changes in terrestrial water storage in the Upper Nile Basin: an evaluation of commonly used gridded GRACE products

M. Shamsudduha et al.

Correspondence to: Mohammad Shamsudduha (m.shamsudduha@ucl.ac.uk)

The copyright of individual parts of the supplement might differ from the CC BY 3.0 License.

Supplementary Table:

Table S1. In each sub sections (LVB and LKB) of the table below, mean annual (2003–2012) amplitudes (first row) and variance (second row) in bottom-up Δ TWS (time-series variance in LVB: 120 cm² and LKB: 24 cm²) explained in linear regression (R^2) by individual signals (third row) such as various GRACE-derived Δ TWS, simulated Δ SMS, in situ Δ SWS and in situ Δ GWS in both and the relative proportion of variability (fourth row) in bottom-up Δ TWS as explained by Δ SMS, Δ SWS and Δ GWS.

Lake Victoria Basin (LVB)					
GRACE Ensemble Δ TWS	GRGS Δ TWS	JPL-MASCON Δ TWS	Δ SMS	Δ SWS	Δ GWS
11.7 cm	20.6 cm	27.3 cm	7.9 cm	14.8 cm	2.9 cm
23.5 cm ²	92.6 cm ²	136.9 cm ²	10.4 cm ²	62.8 cm ²	1.5 cm ²
75%	90%	83%	54%	92%	54%
-	-	-	6.5%	92.6%	0.66%
Lake Kyoga Basin (LKB)					
8. cm	16.2 cm	16.5 cm	7.3 cm	3.8 cm	2.9 cm
11.2 cm ²	58.3 cm ²	47.8 cm ²	7.4 cm ²	4.5 cm ²	2.1 cm ²
62%	56%	57%	62%	48%	76%
-	-	-	48.5%	47.9%	3.6%

Supplementary Figures:

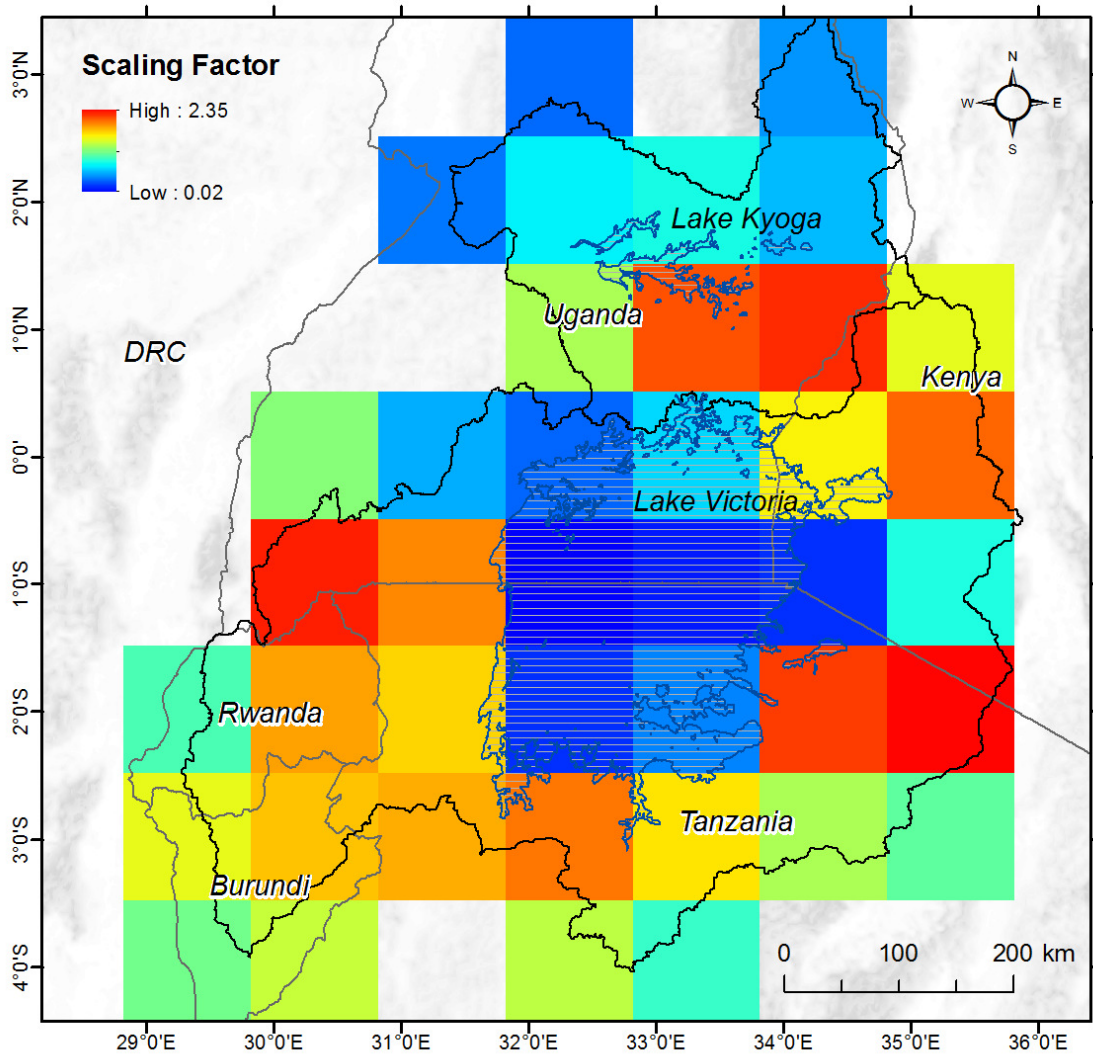


Figure S1. The general outline of Lake Victoria Basin (LVB) and Lake Kyoga Basin (LKB) within the Upper Nile Basin and the gridded ($1^{\circ} \times 1^{\circ}$) scaling coefficients for *GRCTellus* solutions derived from CLM4.0 land surface model (Landerer and Swenson, 2012).

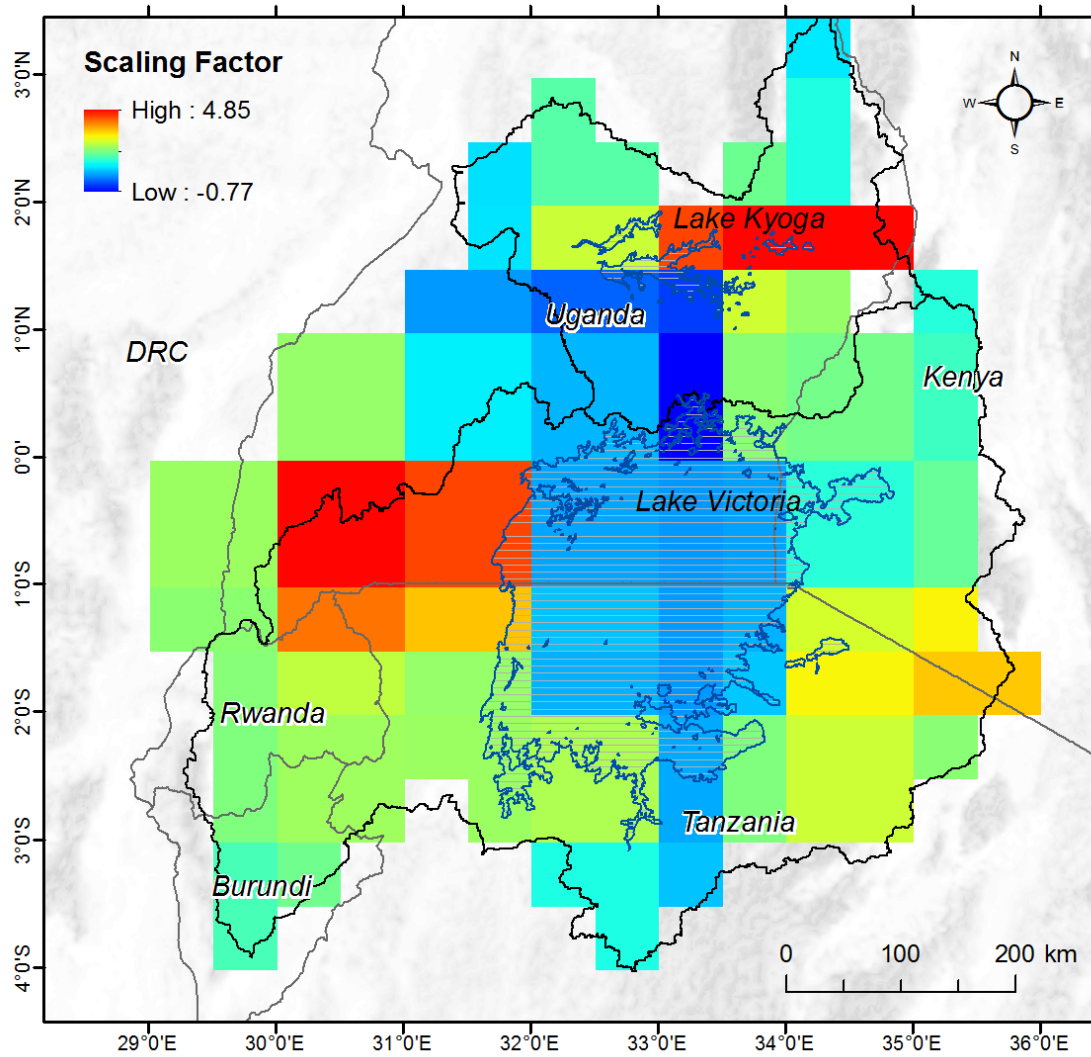


Figure S2. The general outline of Lake Victoria Basin (LVB) and Lake Kyoga Basin (LKB) within the Upper Nile Basin and the gridded ($0.5^\circ \times 0.5^\circ$) scaling coefficients for JPL-Mascons derived from CLM4.0 land surface model (Wiese et al., 2016).

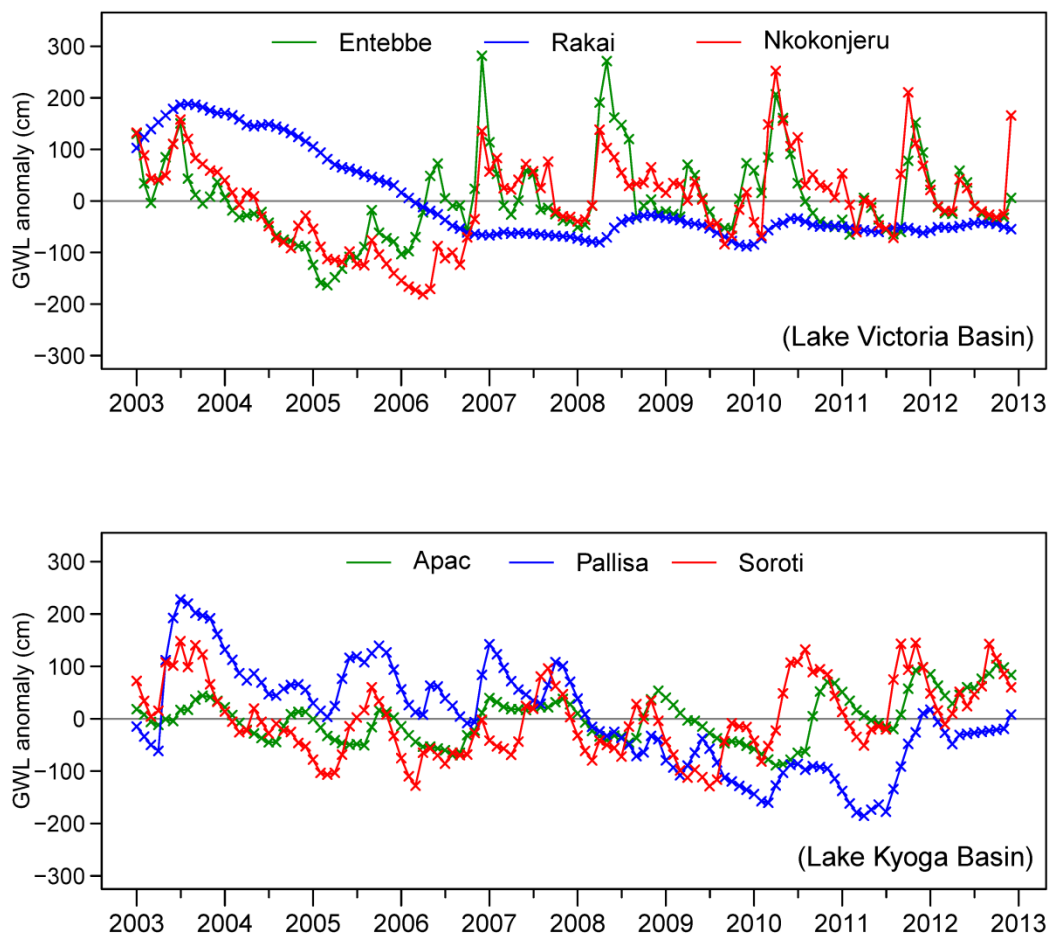


Figure S3. Observed groundwater-level monitoring records (January 2003 to December 2012) at 6 monitoring boreholes: Entebbe, Rakai and Nkokonjeru from Late Victoria Basin (LVB) and Apac, Palissa and Soroti from Lake Kyoga Basin (LKB).

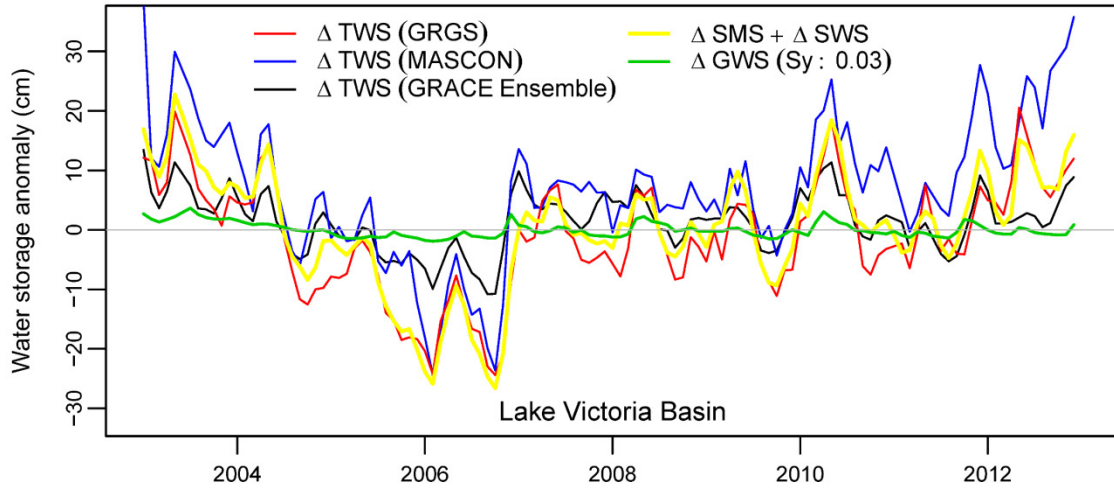


Figure S4. Time-series records of various GRACE Δ TWS solutions, sum of in-situ Δ SWS and ensemble mean of Δ SMS signals and in-situ Δ GWS for Lake Victoria Basin. The graph illustrates that combined signals of Δ SWS+ Δ SMS clearly exceed GRACE Δ TWS anomalies (positive and negative sides of the y-axis) in several monthly instances over the period of 2003 to 2012.

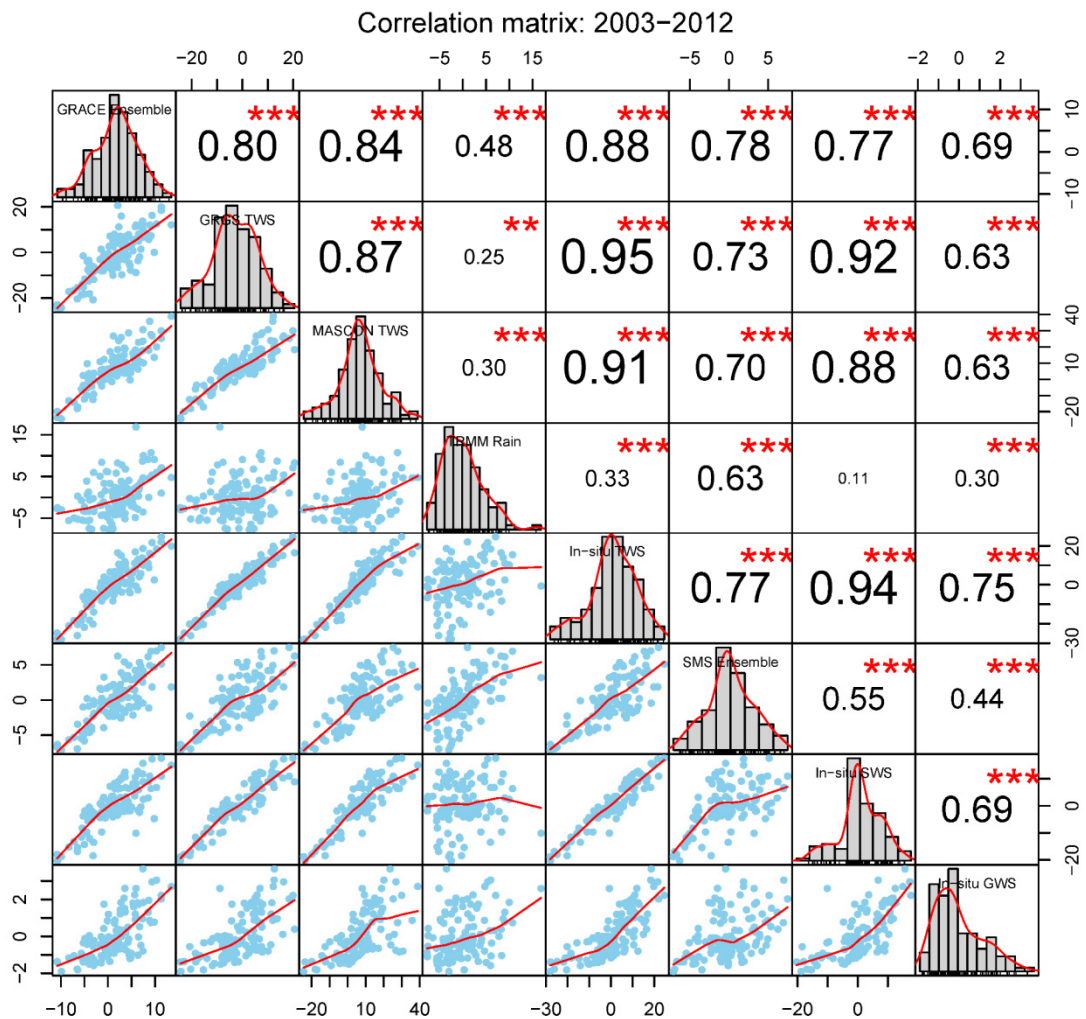


Figure S5. Pearson correlation coefficients among the time-series variables collated over the Lake Victoria Basin for the period of 2003 to 2012. Statistically significant correlated variables are marked with asterisks where the significance asterisks represent p -values < 0.05 (1 asterisk), < 0.01 (2 asterisks) and < 0.001 (3 asterisks). Histograms with kernel density overlays and bivariate scatterplots of variables are shown. The fitted curve lines in bivariate scatterplots represent locally-weighted polynomial regression (i.e., Lowess) lines.

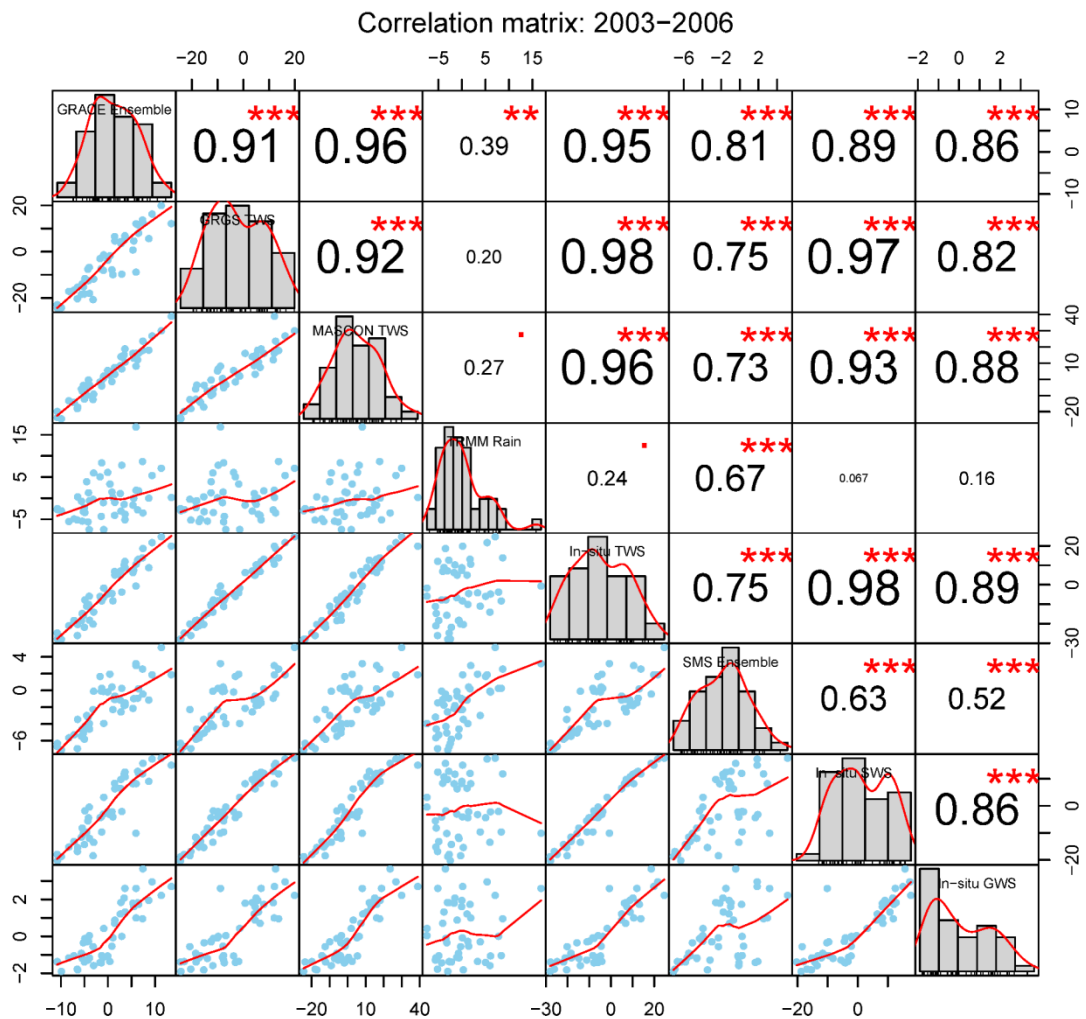


Figure S6. Pearson correlation coefficients among the time-series variables collated over the Lake Victoria Basin for the period of 2003 to 2006. Statistically significant correlated variables are marked with asterisks where the significance asterisks represent p -values < 0.05 (1 asterisk), < 0.01 (2 asterisks) and < 0.001 (3 asterisks). Histograms with kernel density overlays and bivariate scatterplots of variables are shown. The fitted curve lines in bivariate scatterplots represent locally-weighted polynomial regression (i.e., Lowess) lines.

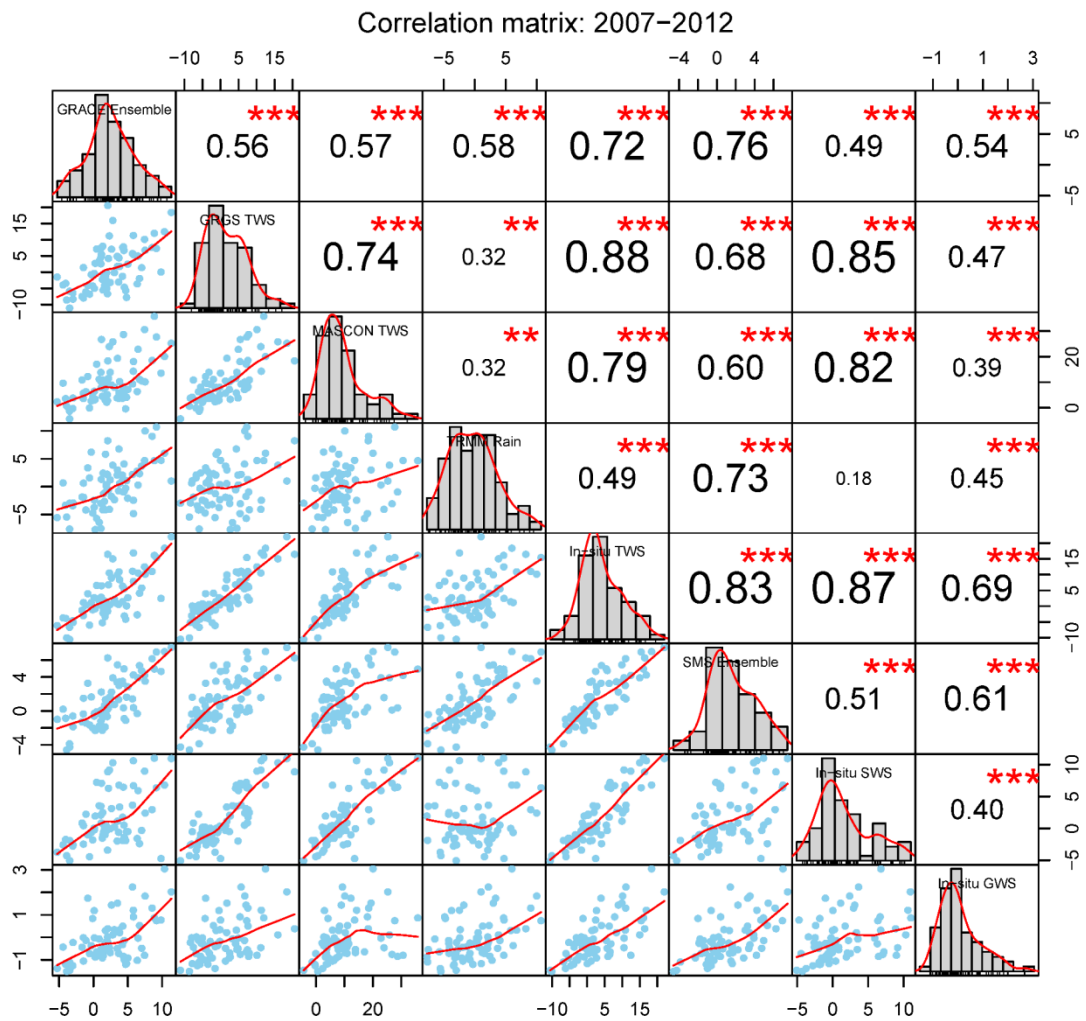


Figure S7. Pearson correlation coefficients among the time-series variables collated over the Lake Victoria Basin for the period of 2007 to 2012. Statistically significant correlated variables are marked with asterisks where the significance asterisks represent p -values < 0.05 (1 asterisk), < 0.01 (2 asterisks) and < 0.001 (3 asterisks). Histograms with kernel density overlays and bivariate scatterplots of variables are shown. The fitted curve lines in bivariate scatterplots represent locally-weighted polynomial regression (i.e., Lowess) lines.

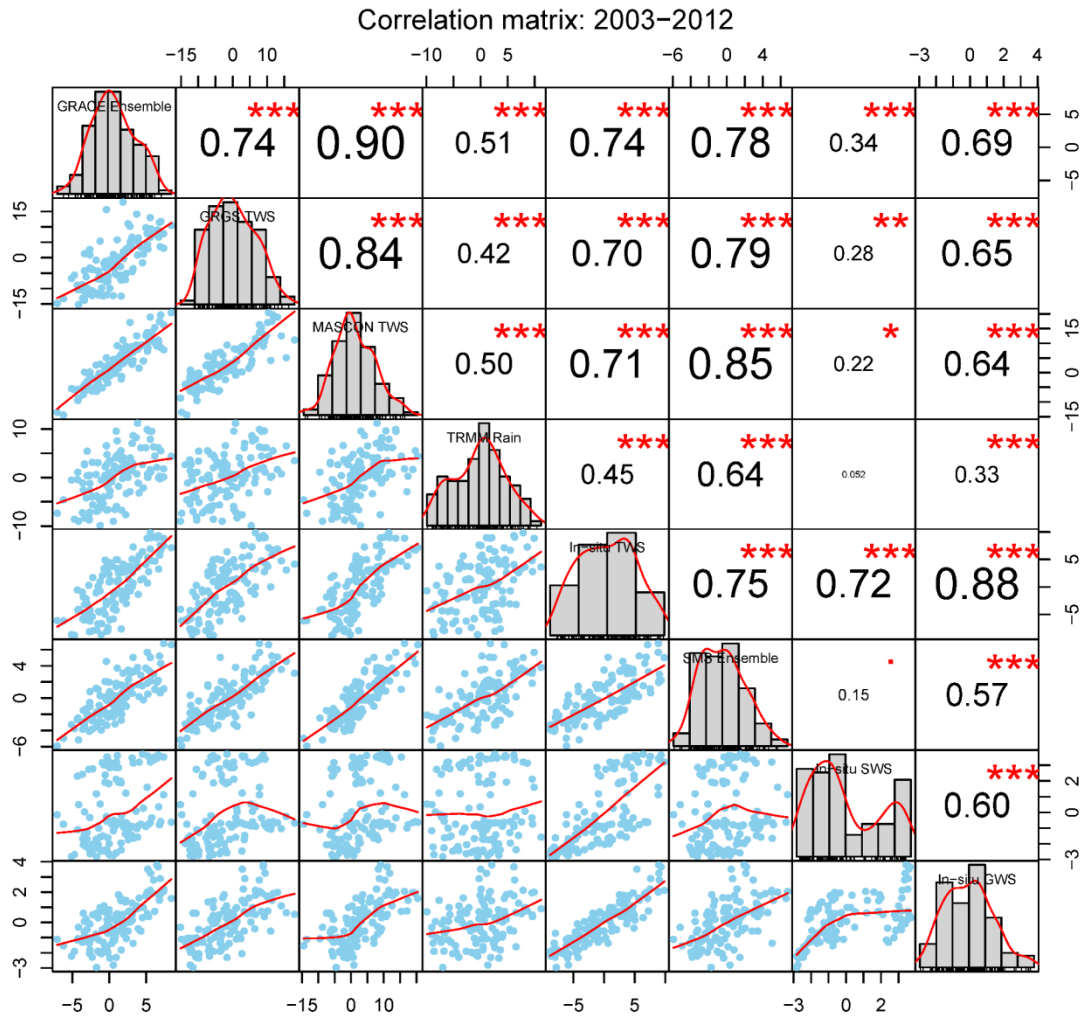


Figure S8. Pearson correlation coefficients among the time-series variables collated over the Lake Kyoga Basin for the period of 2003 to 2012. Statistically significant correlated variables are marked with asterisks where the significance asterisks represent p -values < 0.05 (1 asterisk), < 0.01 (2 asterisks) and < 0.001 (3 asterisks). Histograms with kernel density overlays and bivariate scatterplots of variables are shown. The fitted curve lines in bivariate scatterplots represent locally-weighted polynomial regression (i.e., Lowess) lines.

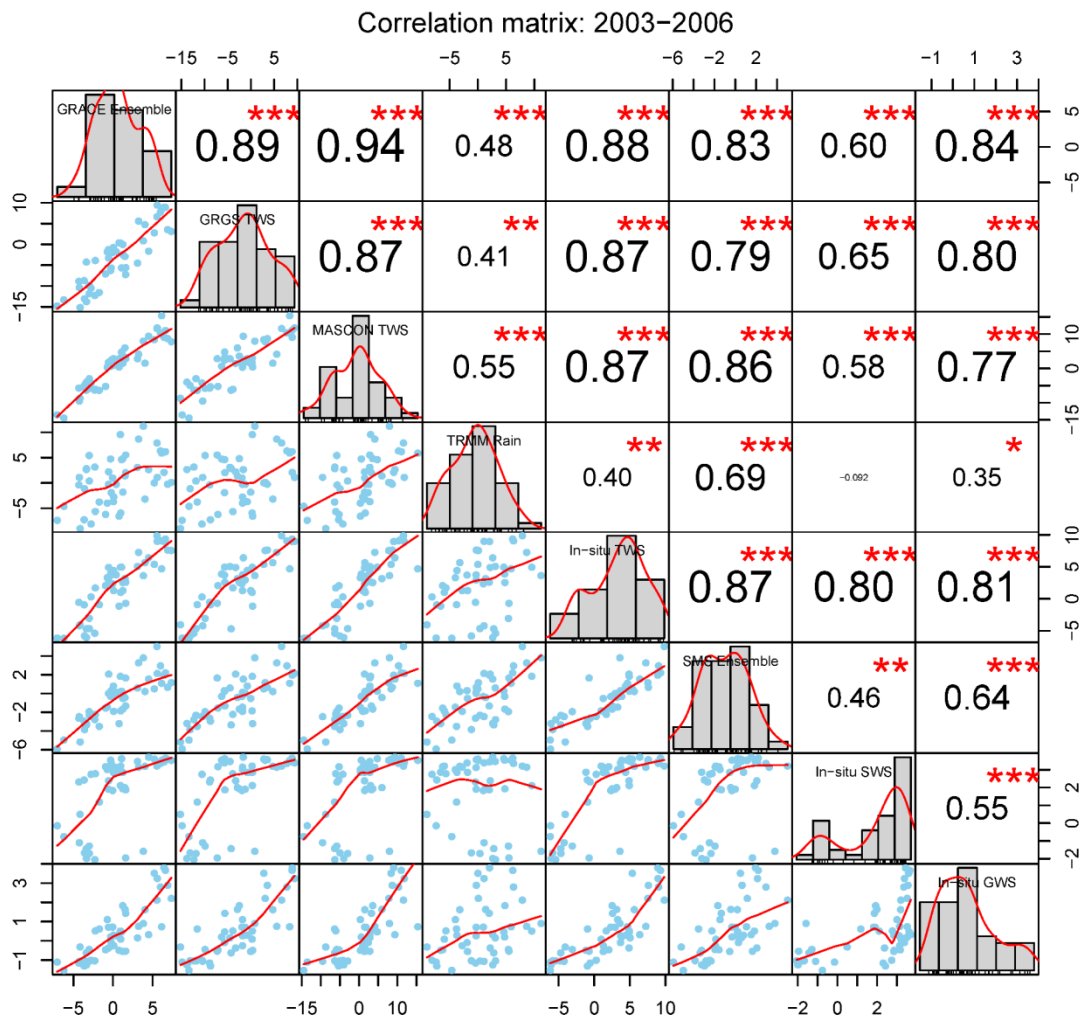


Figure S9. Pearson correlation coefficients among the time-series variables collated over the Lake Kyoga Basin for the period of 2003 to 2006. Statistically significant correlated variables are marked with asterisks where the significance asterisks represent p -values < 0.05 (1 asterisk), < 0.01 (2 asterisks) and < 0.001 (3 asterisks). Histograms with kernel density overlays and bivariate scatterplots of variables are shown. The fitted curve lines in bivariate scatterplots represent locally-weighted polynomial regression (i.e., Lowess) lines.

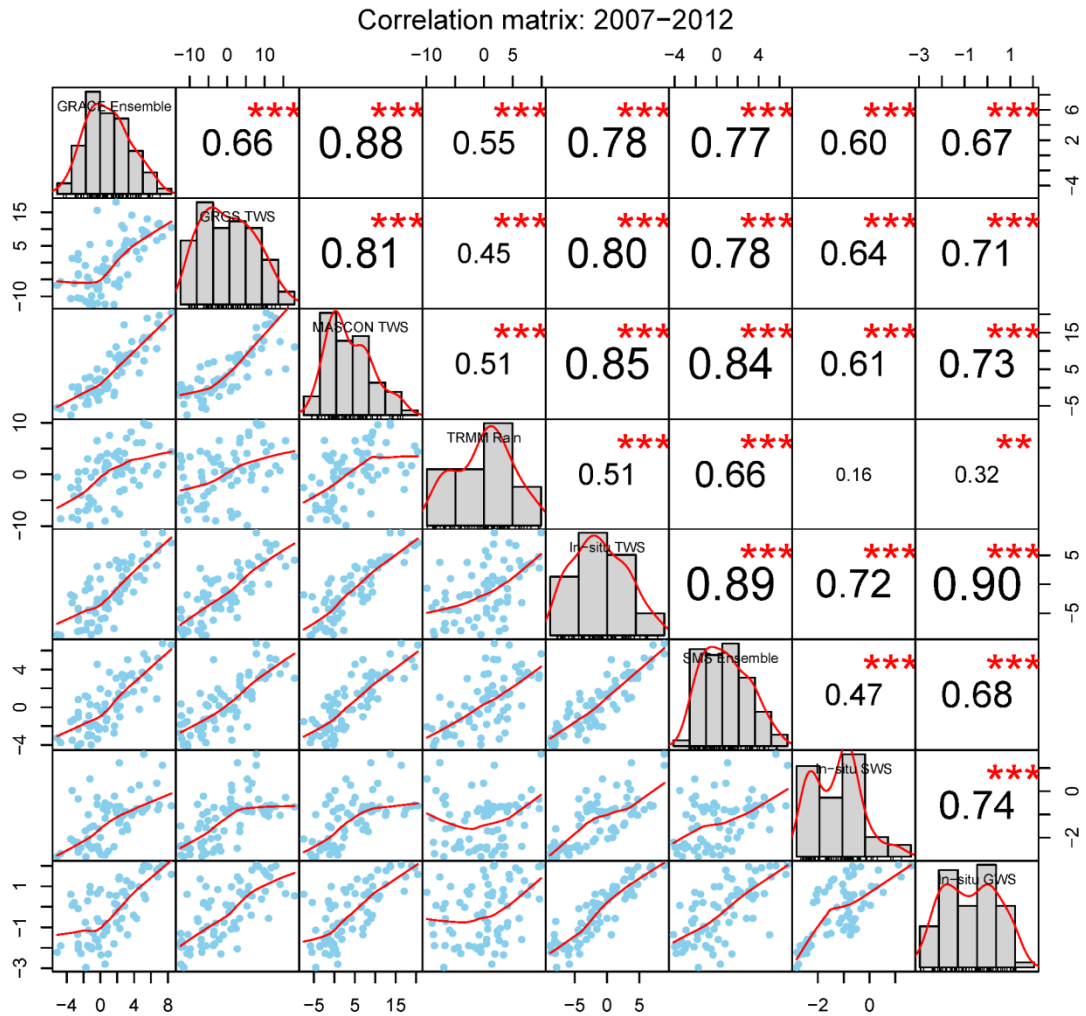


Figure S10. Pearson correlation coefficients among the time-series variables collated over the Lake Kyoga Basin for the period of 2007 to 2012. Statistically significant correlated variables are marked with asterisks where the significance asterisks represent p -values < 0.05 (1 asterisk), < 0.01 (2 asterisks) and < 0.001 (3 asterisks). Histograms with kernel density overlays and bivariate scatterplots of variables are shown. The fitted curve lines in bivariate scatterplots represent locally-weighted polynomial regression (i.e., Lowess) lines.

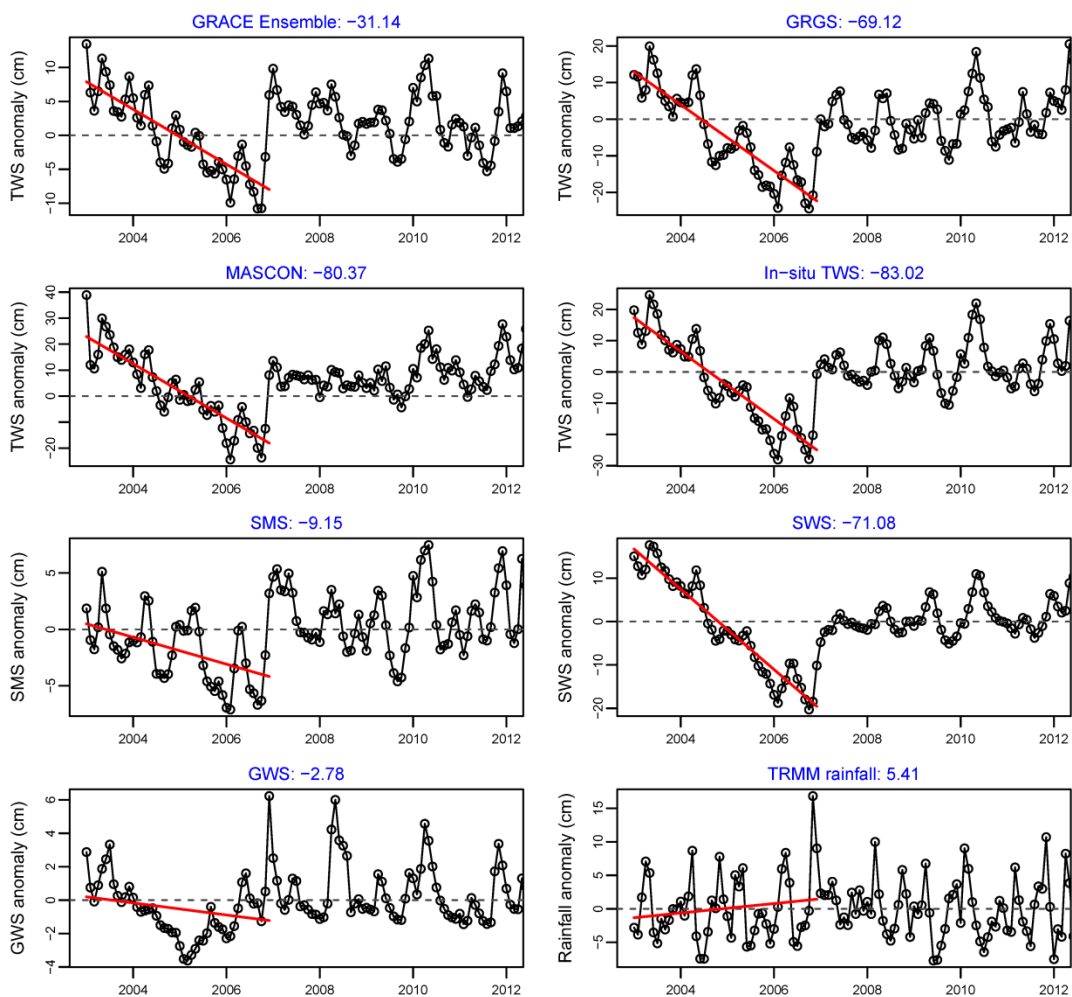


Figure S11. Time-series records of various GRACE Δ TWS signals, in-situ Δ TWS, in-situ Δ SWS, simulated Δ SMS and in-situ Δ GWS in LVB and linear trends (red line) for the period of 2003 to 2006. Figure (blue) on top of each panel indicates the estimated storage change in km^3 .

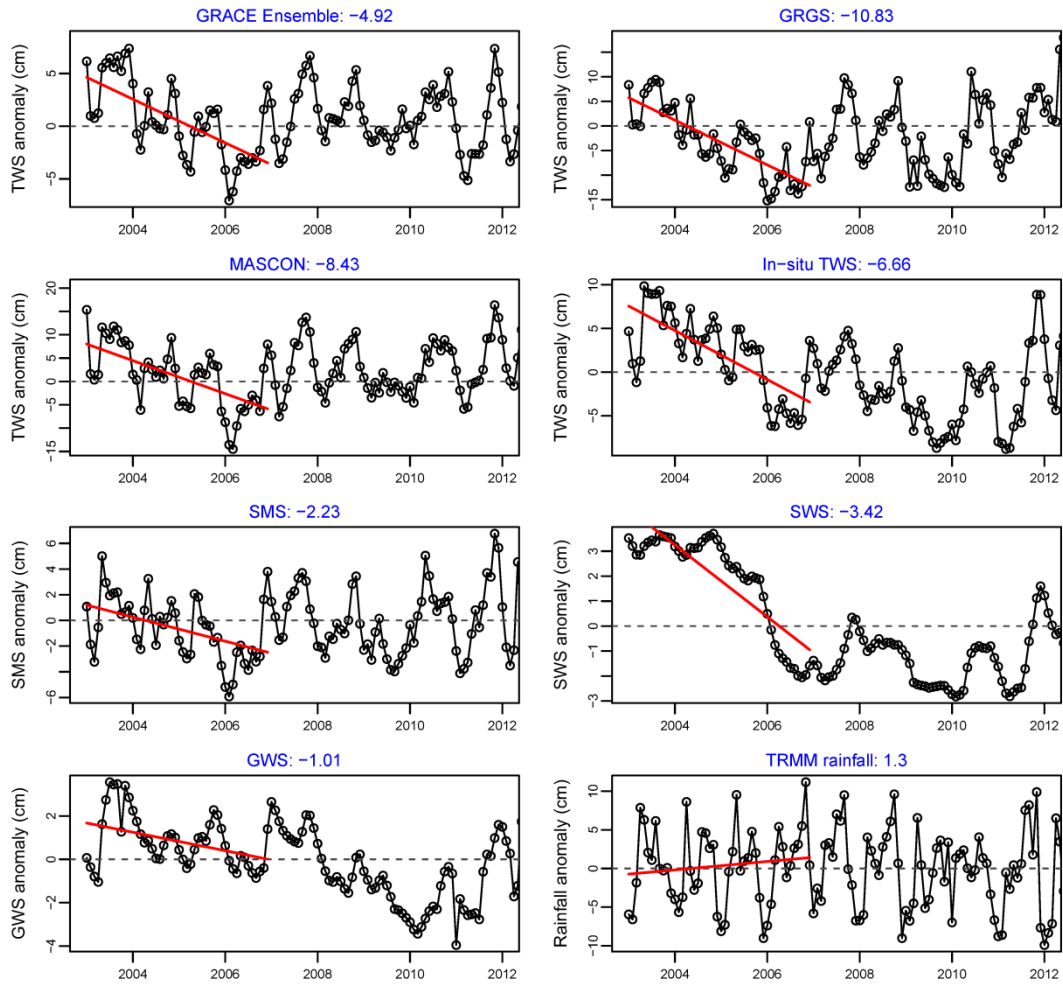


Figure S12. Time-series records of various GRACE Δ TWS signals, in-situ Δ TWS, in-situ Δ SWS, simulated Δ SMS and in-situ Δ GWS in VNB and linear trends (red line) for the period of 2003 to 2006. Figure (blue) on top of each panel indicates the estimated storage change in km^3 .

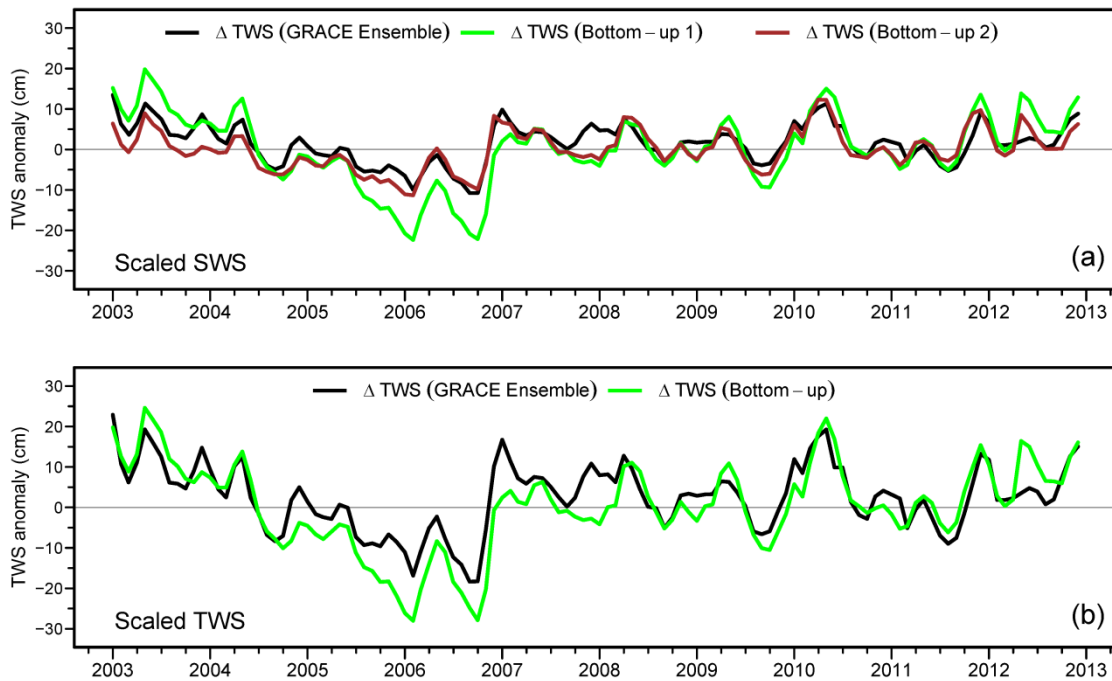


Figure S13. Results of scaling experiments on *GRCTellus* GRACE and in situ Δ TWS over LVB. Panel (a) shows the comparison between *GRCTellus* GRACE-derived Δ TWS and bottom-up Δ TWS where a scaled down (scaling factor of 0.77 bottom-up Δ TWS-1; scaling factor of 0.11 bottom-up Δ TWS-2) Δ SWS signal is applied; on bottom panel (b) shows comparison between *GRCTellus* GRACE-derived Δ TWS and bottom-up Δ TWS where the GRACE- Δ TWS signal is scaled up by a factor of 1.7 based on the lowest RMSE of 5.76 cm with the bottom-up Δ TWS.

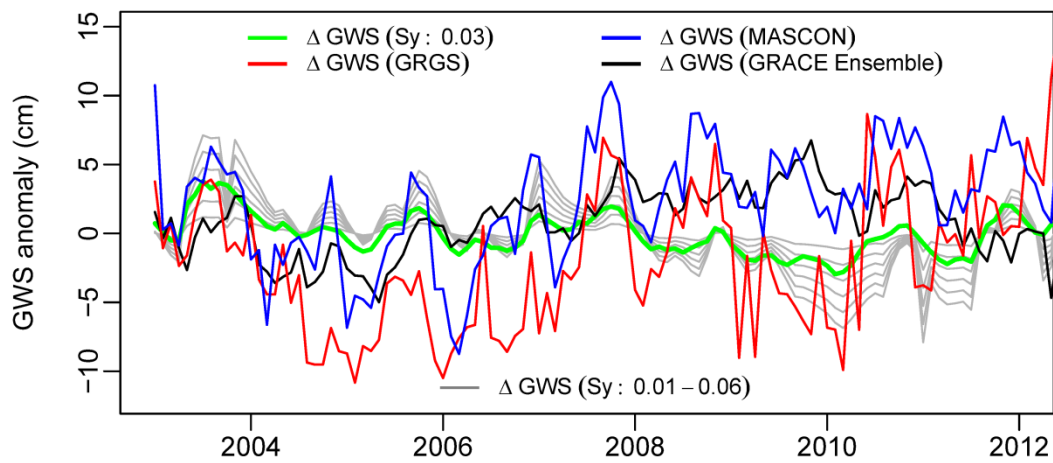


Figure S14. Estimates of in situ Δ GWS and GRACE-derived Δ GWS time-series records (2003–2012) in LKB show a substantial variations among themselves. No scaling experiments were applied for LKB in the disaggregation of Δ GWS using *GRCTellus* (ensemble mean of CSR, GFZ, and JPL) and JPL-Mascons GRACE products.

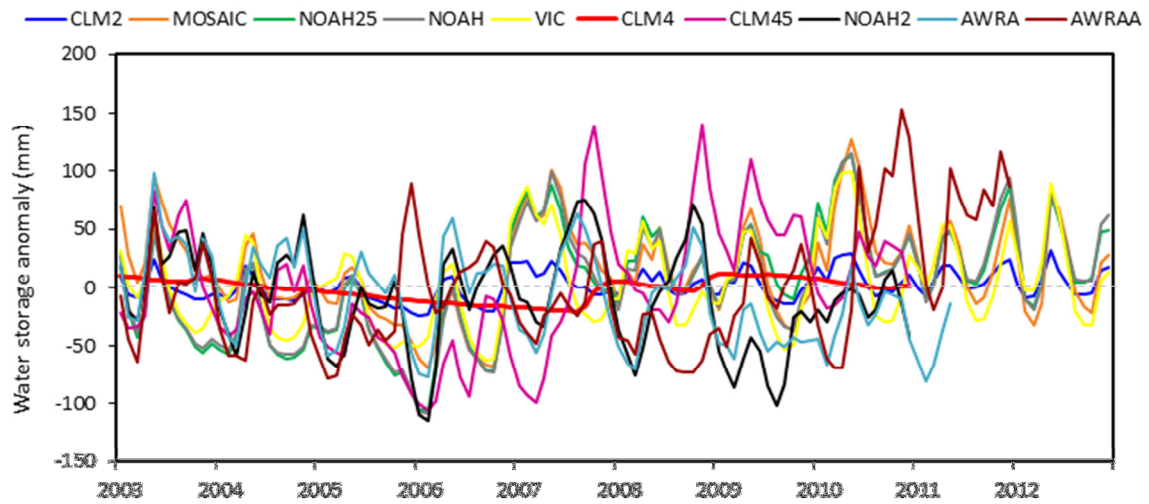


Figure S15. Simulated terrestrial water storage anomaly from 10 LSMs for the Lake Victoria Basin. Note that not all LSMs simulate groundwater storage; for example, latest versions of the Community Land Model (CLM4.0 and 4.5) simulate groundwater storage.